Journal of Electrochemical Science and Technology

Electrocatalytic Oxidation of HCOOH on an Electrodeposited AuPt Electrode: its Possible Application in Fuel Cells

Sunghyun Uhm[a], Hongrae Jeon[b] and Jaeyoung Lee[a,b,†]

[a]Ertl center for Electrochemistry and Catalysis
[b]Electrochemical Reaction and Technology Laboratory (ERTL), School of Environmental Science and Engineering, Gwangju Institute of Science and Technology, Gwangju 500-712, South Korea

ABSTRACT :

Controlled electrodeposition of dendritic nano-structured gold-platinum (AuPt) alloy onto an electrochemically pretreated carbon paper substrate was conducted in an attempt to improve catalyst utilization and to secure an electronic percolation network toward formic acid (FA) fuel cell application. The AuPt catalysts were obtained by potentiostatic deposition. AuPt catalysts synthesized as bimetallic alloys with 60% Au content exhibited the highest catalytic activity towards formic acid electro-oxidation. The origin of this high activity and the role of Au were evaluated, in particular, by XPS analysis. Polarization and stability measurements with 1 mg cm^{-2} AuPt catalyst (only 0.4 mg cm^{-2} Pt) showed 52 mW cm^{-2} and sustainable performance using 3 M formic acid and dry air at 40°C.

Keywords : electrodeposition, AuPt alloy, dendritic nanostructure, formic acid fuel cells.

1. Introduction

Small organic molecules (SOM) such as methanol, formic acid, formate, and ethanol have great potential as possible fuels in direct small organic fuel cells.[1-10] Among them, formic acid is a liquid at room temperature and dilute formic acid is on the US FDA list of food additives that are generally considered as safe. In concentrated form however, it needs to be handled with appropriate care. Furthermore, even though formic acid has only about half the energy density of methanol,[6] a direct formic acid fuel cell (DFAFC) has a higher power density compared with a direct methanol fuel cell (DMFC) by virtue of its lower fuel crossover rate through the polymer electrolyte and faster oxidation kinetics of formic acid on anode catalysts.[11,12]

The largest contributing cost to a DFAFC is the signifi-

†Corresponding author. Tel.: +82-62-970-2440
 E-mail address: jaeyoung@gist.ac.kr

cant amount of platinum metal group (PMG) catalyst necessary for high power (typically from 2-8 mg cm^{-2} for only the anode).[13-16] Unfortunately this cost is only expected to increase as the global demand for Pt increases. Until now, in spite of the problem of being strongly poisoned by intermediate species, Pt is the best known catalyst for the oxidation of small organic molecules if the catalytic activity and stability are considered simultaneously. Although Masel et al. reported that Pd possesses unusually high activity for the electro-oxidation of formic acid, its stability is relatively poor and it can not run for more than a few hours without loss of its activity by ca. 50% depending on the operating conditions.[15-17] This is a clear demonstration that the presence of Pt is strictly necessary in the catalyst composition.

Fortunately, binary Pt alloy catalysts have been discovered to use less Pt and to alleviate the loss of activity by strong poisoning. Accordingly, one of the requirements for the second metal would be an ability to suppress the formation of poisonous species absorbed on more than

one surface active site, so-called ensemble effects.[18] The most promising candidate possessing such ensemble effects for formic acid electro-oxidation is gold (Au). In spite of the lower electrocatalytic activity of Au compared to Pt, formic acid oxidation on pure Au as well as AuPt alloy electrodes has been extensively investigated.[19-23] AuPt nanoparticles might provide a synergistic catalytic effect that involves the suppression of adsorbed poisonous species and a change in electronic band structure to modify the strength of the surface adsorption because, unlike at a Pt electrode, the self-poisoning phenomena do not occur at the Au electrode. In other words, one could explore the viability of using Pt as the main dehydrogenation sites and Au along with Pt to speed up the removal of poisoning species.

Along with the chemical and electrochemical nature of the components, the preparation method is another essential feature in the development of catalysts as well as electrodes.

Catalysts used in direct formic acid fuel cells are usually prepared in the form of black (unsupported) nanoparticles in order to reduce ohmic drop, mass transport and manufacturing problems deriving from the use of thick electrodes.[22,23] However, the presence of catalyst agglomeration effects in black catalysts significantly limits their utilization in fuel cell systems. Basically, the catalyst (e.g. Pt) must have simultaneous access to the fuel (gas or liquid), the electron-conducting medium (carbon or metal itself), and the proton conducting medium (ionomer) in order to effectively utilize the Pt catalyst. However, even in the catalyst layer prepared by most advanced conventional electrode preparation process (generally ink based process), there is still a significant portion of Pt that is inevitably isolated from the external circuit because of the addition of ionomer for proton transport. Estimates from the percolation theory suggest that even for a best architecture of the catalyst layer, electrochemically active surface fractions of Pt comprise ~40% of the total Pt surface.[24,25] As a direct deposition technique for higher catalyst utilization, the electrodeposition of noble metal catalysts in desired locations has attracted much attention due to its relative simplicity and the low cost process.[26-35] However, it is still very hard to achieve relatively high metal loading (e.g., 1-2 mg cm^{-2}) along with controlled small particle size especially for a direct liquid fuel cell anode and there are impurity problems in the catalyst layer after electrodeposition since ionomer-carbon composite material is used as substrate.

The scope of the present study is to look for a way to fabricate AuPt alloy catalyst (or electrode) by electrodeposition along with improved catalyst utilization toward formic acid fuel cell application. The electrodeposition of AuPt alloy catalyst was conducted directly on the pretreated plain carbon paper for better electronic percolation network. The electrochemical and morphological nature of a nanostructured AuPt catalyst was characterized together with the composition and electronic state of surface region. Lastly, feasibility tests with home-made AuPt catalyst were carried out for direct formic acid fuel cells by current-voltage polarization measurement.

2. Experimental

2.1. Preparation of electrodes by electrodeposition

The SGL plain carbon paper (®SIGRACET GDL 25AA, 190 μm in thickness, ca. 50 g m^{-2} in a real weight and BET surface area < 1 m^2 g^{-1}, SGL CARBON JAPAN LTD) was used as electrochemically oxidized in order to improve the dispersion of electrodeposited catalysts and intrinsic catalytic activity.[36,37] For the electrochemically oxidized electrodes, samples were cut to the required size and installed in a teflon holder. They were then immersed in 0.5 M HClO$_4$. A constant potential of 2.0 V (*vs.* Ag/AgCl) was applied for 2 min with an Autolab PGSTAT30 (Eco Chemie) potentiostat/galvanostat with conventional experimental apparatus consisting of a three electrode cell setup using an Ag/AgCl reference electrode and a Pt wire counter electrode. All solutions were prepared with ultrawater (Millipore Milli-Q water, 18 MΩ cm) and purged with N$_2$ gas before and during each experiment. The geometric area of the electrode samples exposed to electrolyte for the half-cell test and membrane electrode assembly (MEA) was 0.8 and 9 cm^{-2}, respectively.

Following the electrochemical oxidation process, Pt and AuPt catalyst were electrodeposited on the as-prepared carbon paper substrate with the plating solutions shown in Table 1. The total concentration of active species was 10 mM. Each cell was filled with 250 ml of a solution containing H$_2$PtCl$_6$, HAuCl$_4$ (Sigma), Pb(CH$_3$COO)$_2$ (Junsei), and HClO$_4$ (Aldrich) as a supporting electrolyte. 0.2 mM Pb(CH$_3$COO)$_2$ was added as an additive for black nanoparticles.[38,39] Depositions were carried out potentiostatically at 0 V (*vs.* Ag/AgCl), which was selected

Table 1. The precursor molar ratio in individual plating solutions

Samples	H$_2$PtCl$_6$: HAuCl$_4$
Pt	10 : 0
AuPt(I)	5 : 5
AuPt(II)	3 : 7

to produce highly defective nanostructured particles.[40] The loading of deposited metal was calculated and controlled by the total charge applied. The actual current efficiency was ca. 46% for Pt and 50-52% for AuPt by way of weighing the electrode before and after the electrodeposition.

2.2. Characterization of electrodes

After the electrodeposition process, cyclic voltammograms (CVs) were recorded at 50 mV s^{-1} in 0.5 M HClO$_4$ and at 10 mV s^{-1} in 0.5 M HCOOH (Jusei) and 0.5 M HClO$_4$ supporting electrolyte. After the electrochemical measurements, the electrodes were removed for morphology and surface property analysis. After the electrochemical measurement and before the surface analysis procedures, the electrolyte was leached from the samples using DI water, and dried in an oven at 60ºC under atmospheric conditions. Structural analyses of Pt and AuPt alloy catalysts were carried out using a high resolution X-ray diffractometer (HR-XRD, D/MAX Ultima III). The surface morphology was characterized with a field emission scanning electron microscope (FE-SEM, Hitachi S-4700). The composition and electronic state of the surface region was analyzed using X-ray photoelectron spectroscopy (XPS, VG Multilab 2000) and energy dispersive X-ray spectroscopy (EDX, Horiba). For calibration of the energy scale the reference energies assumed were C1 s (284.4 eV) and Au4f7/2 (83.9 eV).

2.3. Membrane electrode assembly and performance test

The membrane electrode assemblies (MEAs) were prepared as follows: the anode consisted of as-prepared Pt or AuPt electrode impregnated with Nafion solution (Aldrich, 5 wt%). The ionomer content in the catalyst layer was 0.5 mg cm^{-2}. The cathode consisted of carbon paper as a substrate (SGL 35BC GDL) onto which Pt black (Johnson Matthey, 3.0 mg cm^{-2}) was loaded with 10 wt% Nafion solution. The electrodes were placed on either side of a Nafion 115 membrane. The assembly was hot-pressed at 10 MPa for 5 min at 140ºC.

The resulting MEA, with an electrode area of 9 cm^{-2}, was sandwiched between two graphite blocks having serpentine flow path channels. The cell temperature was maintained at 40ºC and 3 M formic acid aqueous solution and dry air were applied at flow rates of 5 cc min^{-1} and 200 sccm, respectively. Current-Potential transients were measured using an electronic load.

3. Results and Discussion

Fig. 1 shows the morphologies of the Pt and AuPt catalyst electrodeposited on the fibers of plain carbon paper with 0.5 mg cm^{-2} metal loading. Unlike the pure Pt in Fig. 1(a), Figs. 1(b) and (c) are SEM images of some
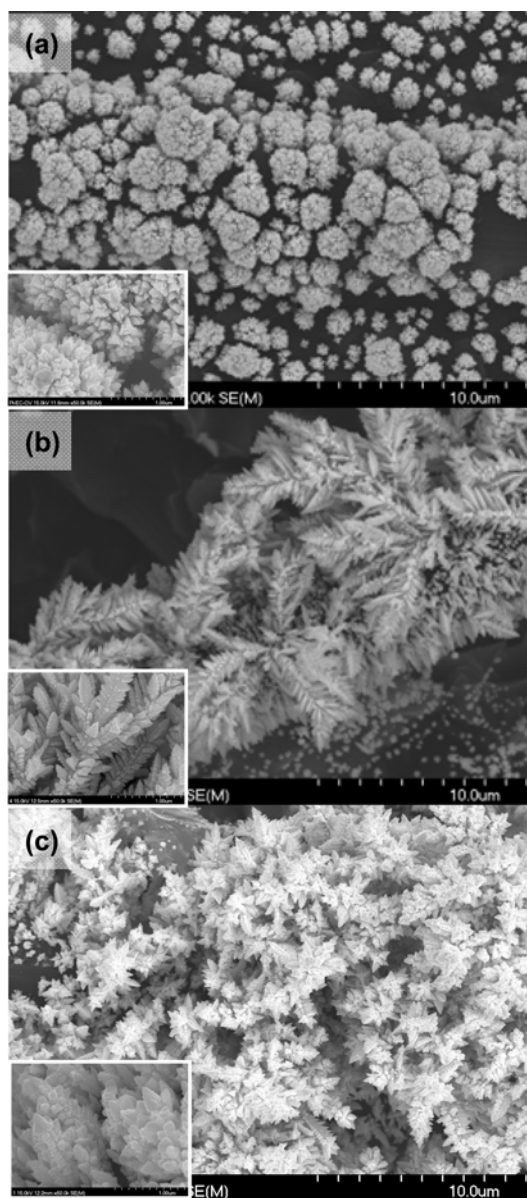
Fig. 1. SEM images (5,000x) showing Pt (a), AuPt(I) (b) and AuPt(II) (c) electrodeposited on carbon paper with 0.5 mg cm^{-2}. Inserts are more highly magnified images (50,000x) of each nanoparticle.

typical dendrites, showing that the individual dendrite composed of almost symmetrical branches and leaves is about 2-5 μm in length. Moreover, the dendritic heteroaggregate nanostructure becomes predominant as the Au content of the plating solution is increased (Fig. 1(c)). Many nanoparticles aggregate to nanocrystals, and as these grow, the dendritic heteroaggregate nanostructures form gradually. Due to the screening effects, some parts of the dendrites can always take up AuPt nanoparticles and become larger and larger; others however cannot and stop growing at an early stage.

The alloy characteristics for both the surface and the core of the carbon paper supported Pt and AuPt catalysts were also characterized by XRD measurements. Shown in Fig. 2 are the X-ray diffraction patterns of Pt and AuPt(I) and (II) samples. Pt samples showed clear reflections at angles of 39.8, 46.2, 67.4, 81.2 and 85.7° that are associated with the [111], [200], [220], [311] and [222] facets of Pt crystallites, respectively.[41,42] On the other hand, the XRD pattern of AuPt(I) and AuPt(II) exhibited diffraction lines, which are located between the corresponding diffraction peaks of the two corresponding monometallic nanoparticles. The equivalent facets of Au crystallites are connected with reflections at the angles of 38.2, 44.4, 64.6, 77.5 and 81.7°, respectively.[43-45] This strongly suggests the formation of an alloy structure. As expected, with an increase of Au content of plating solutions, clear peak displacements into more Au-like pattern were observed. The reflection at angle of 54.5° corresponds to graphitic carbon. Assuming alloy formation between Pt and Au based on a substitutional solid solution, such a shift can be attributed to the difference in atomic size [46]. There-
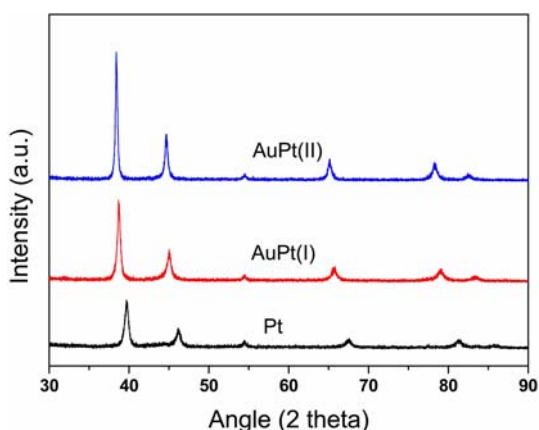

Fig. 2. XRD patterns of Pt and AuPt alloy catalyst electro-deposited on carbon paper.

fore, the higher the content of Au in an alloy becomes, the more peak shifts occurs. The particle size of synthesized nanoparticles can be calculated using the Debye-Scherrer equation by fitting the [220] peak.[23] The average size of synthesized Pt, AuPt(I) and AuPt(II) nanoparticles are 14, 12 and 19±3 nm, respectively. This is in good agreement with agglomeration behavior due to higher content of Au as shown in the SEM image of Fig. 1(c). Usually, the Pt particle sizes from electrodeposition fall in the range of 20-70 nm unless the Pt loading is ultralow (i.e., 0.05 mg cm^{-2}).[47,48] This indicates that the Pt and AuPt nanoparticles synthesized in this study have well dispersed and relatively small particle sizes. In particular, the particle size of the AuPt(I) catalyst is the smallest among samples due to its typical dendritic morphology.

XPS is very surface sensitive tool and can provide information about the composition and electronic state of the surface region. Fig. 3 shows the XPS spectra of Pt and AuPt particles as a function of the varying amounts of Au. In Fig. 3(a), a remarkable weakening of the Pt4f signals at 70.8 and 74.0 eV is accompanied by the appearance and strengthening of the Au4f signals at 83.9 and 87.5 eV with an increase of Au content. We measured the atomic Pt/Au ratio at the surface of AuPt nanoparticles (Table 2) using the Au and Pt XPS signals combined with EDX (TEM) analysis. The Au content is about 60 wt% for AuPt(I) and increases up to about 80 wt% for AuPt(II) according to both analyses coincidentally. This result indicates that $[AuCl_4]^-$ is reduced earlier than $[PtCl_6]^-$, as can be understood by considering the redox potentials of the two precursor ions in Table 1.[49]

The binding energies and relative intensity (the sum of both 4f7/2 and 4f5/2 peak areas) of the Pt and PtO species present in different Au content were evaluated by deconvolution of the spectra in Figs. 3(b)-(d). The lower binding energy doublet with Pt4f7/2 at 71.1 eV can be assigned to zero-valent Pt.[50,51] In contrast, the higher binding energy doublet at 72.0 eV is close to the chemical shift reported for PtO.[50] In fact, the relative intensity of the PtO doublet is considerably lower than that of the native metal signal in every spectrum. However, the relative intensity becomes larger with an increase of Au content, indicating the presence of Pt atoms at sites with poor metallic coordination and consequent high oxygen coordination.[52] Furthermore, although the Pt4f7/2 spectra of AuPt nanoparticles have similar binding energy to those of pure Pt nanoparticles, we find a definite negative shift of ca. 0.3 eV in the binding energies of all deconvoluted species for both AuPt alloy catalysts in relation to those observed
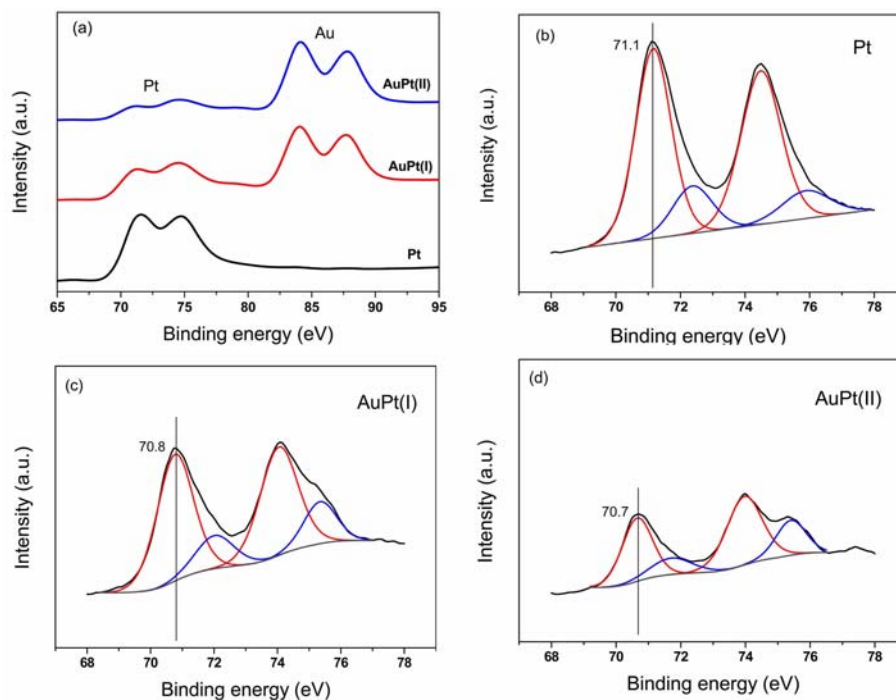
Fig. 3. XPS spectra of Pt4f and Au4f region during data acquisition (a) and XPS of core-level region of Pt4f in pure Pt (b), AuPt(I) (c) and AuPt(II) (d).

**Table 2.** Surface Pt atomic ratio with respect to Au of samples determined by XPS and EDX

Samples	XPS	EDX
AuPt (I)	0.65	0.63
AuPt (II)	0.25	0.28

for pure Pt systems. This can be interpreted by chemical interaction between Pt and Au, which increases the binding energy if Pt atoms act as electro donors or decreases the binding energy if they act as electron acceptors.[53,54] This suggests the occurrence of charge transfer from Au to Pt nanoparticles in AuPt nanoparticles. A lower Pt4f7/2 binding energy reflects the higher electron density in the vicinity of the Pt atoms due to the charge transfer from Au to the Pt atoms. This property may result from the distinct electronic structure or significant surface effects due to their dendritic nanostructures.

One of the important parameters for Pt-based electrocatalysts is the electrochemical active surface area, which is generally calculated using the hydrogen desorption peaks on the well-known CV curves measured in acidic media.

Fig. 4(a) shows the CV curves in 0.5 M $HClO_4$ on carbon paper supported Pt and AuPt nanoparticles. In agreement with the property of an Au electrode in acidic media,[55] AuPt alloy catalysts showed very depressed H adsorption/desorption and Pt oxidation/reduction features with increased Au content. Thus, the depressed features of AuPt alloy catalysts may be associated with the transformation into a more Au-like character.

All of the as-prepared electrocatalysts were further evaluated for the electro-oxidation of formic acid. Fig. 4(b) shows the CV curves of home-made Pt and AuPt alloys in 0.5 M HCOOH and 0.5 M $HClO_4$ at a scan rate of 10 mV s^{-1}. On the anodic scan, Pt catalyst shows typical two peaks in which the first peak around 0.5 V is due to the direct oxidation of HCOOH on the remaining sites unblocked by intermediate CO_{ads} and the second anodic peak is related to the oxidation of CO_{ads} that releases the surface sites for the subsequent direct oxidation of HCOOH.[56,57] On the other hand, AuPt alloy catalysts exhibit superior formic acid electro-oxidation of 37.5 and 35.4 mA cm^{-2} for AuPt(I) and AuPt(II) at 0.2 V (vs. Ag/AgCl) near the kinetically controlled potential region, compared to ca. 10 mA cm^{-2} for Pt catalyst. Instead they
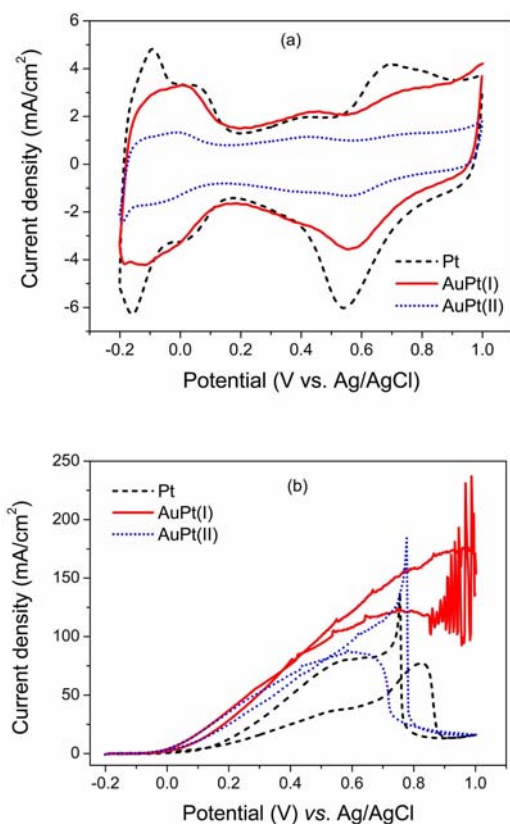
Fig. 4. Cyclic voltammograms in 0.5 M HClO$_4$ at a scan rate of 50 mV s^{-1} (a) and in 0.5 M HCOOH + 0.5 M HClO$_4$ at a scan rate of 10 mV s^{-1} (b).

showed rather an unusual wavelike increase of current and eventual oscillation for AuPt(I) and earlier fall-down of current for AuPt(II) than any distinct two-step peaks. However, a too high Au content in AuPt alloy catalyst has no positive effects on formic acid electro-oxidation due to either lack of dehydrogenation sites (decreased Pt content) or higher oxygen coordination of Pt as described above (XPS characterization). The remarkably higher oxidation current and considerably lower onset potential of the AuPt alloy catalyst is directly related to the facts that Au atoms alloyed with Pt atoms in the AuPt alloy catalyst may have played an important role in either eliminating the formation of the intermediate CO-like species or providing oxygenated species more favorably for the complete electro-oxidation of formic acid.[58] Another remarkable result is that only 20-40% Pt was present in the AuPt catalyst systems. Accordingly, the superiority of the electrocatalytic activity for the bimetallic AuPt alloy catalyst with 60-80% Au compared to those for pure Pt catalyst is suggestive of the participation of

Au in the catalytic reaction of Pt, presenting bifunctional electrocatalytic property by strong alloy formation.

In general, the final criterion for well-prepared catalysts is its successful application to the electrodes in an actual fuel cell system consisting of polymer membranes and electrodes (catalyst powder and ionomer mixture). The catalyst layer or electrode was depicted as starting from the microstructural model proposed by Uchida et al.[59,60] and implemented with concepts of the percolation model for porous electrodes.[61,62] All catalysts would be well dispersed on the outer agglomerate surfaces for higher utilization. These surfaces would be covered with electrolyte fraction so that they would all be accessible to protons. Additionally, in the case of a cathode, the catalyst layer should be hydrophobized enough to obtain good oxygen accessibility and to avoid blocking effects due to flooding of pores with product water. In several aspects of the description given above, the improvement of one property could have a negative effect on other properties. Thus, identifying optimum performance is, evidently, a matter of tuning the compositional and structural parameters of the catalyst layers.

In view of its percolation network, the carbon paper electrode assures a close to perfect electronic conduction, if the ionic conduction could be improved. Fig. 5 shows SEM images of AuPt(I) catalysts electrodeposited directly on the carbon paper to ensure an adequate catalyst layer with respect to catalyst loading. Due to the very porous and low-density structure of carbon paper, relatively high metal loadings should be achieved. However, a much thicker catalyst layer with 1.5 mg cm^{-2} as shown in Fig. 5(e), might, on the contrary, hinder the simultaneous formation of three interpenetrated percolating of electrical conduction, ionic conduction and fuel supply channel. Furthermore, the agglomeration can be accelerated with an increase of metal loading since a simple potentiostatic method was utilized to prepare catalysts due to the probability of Ostwald ripening process.[29]

Fig. 6(a) shows the polarization curves at 40°C using MEA prepared with electrode of Fig. 5(d), which is well optimized with respect to tuned catalyst loading and ionomer content in the catalyst layer. For comparison, Pt electrode was prepared with a similar procedure with same metal loading of 1.0 mg cm^{-2}. It is well known that at low temperature, the catalysts have a dominating effect on the performance of fuel cells without effects of transfer phenomena of reactants and products. Around 0.5 V where an activation polarization dominates the activity of the catalyst, the current density of AuPt(I) catalyst is about three times
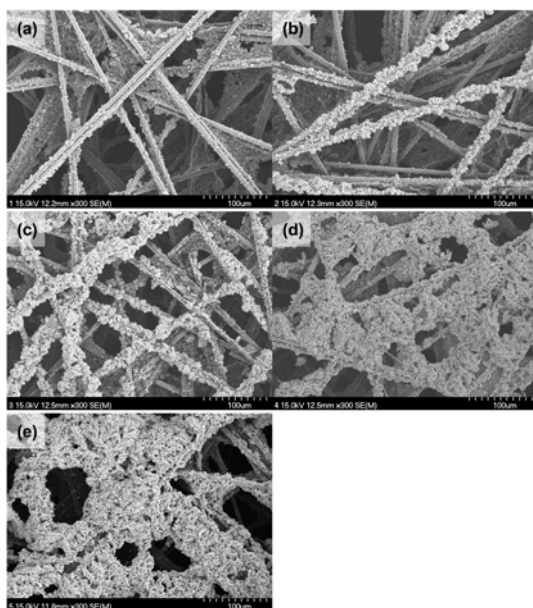
Fig. 5. SEM images of AuPt(I) electrodeposited on carbon paper with different metal loading. (a) 0.1, (b) 0.3, (c) 0.5 (d) 1.0 and (e) 1.5 mg cm^{-2}.
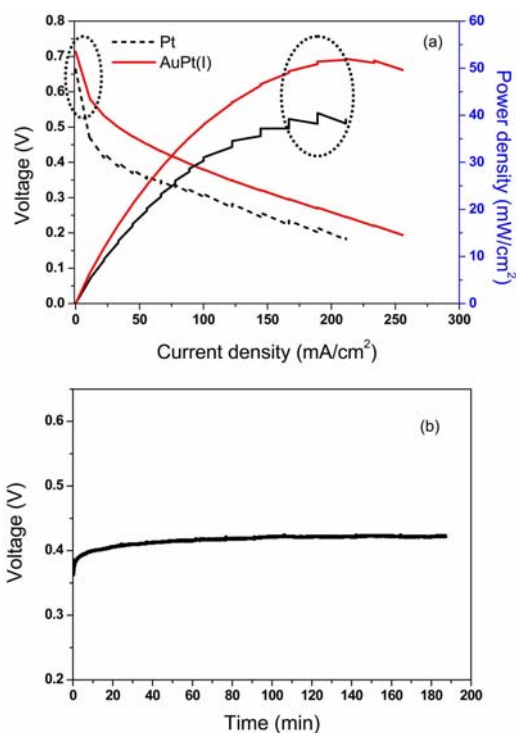

Fig. 6. Polarization curves for a direct formic acid fuel cell at 40°C with 3 M formic acid and dry air without back pressure (a) and voltage variation with a function of time at 100 mA cm^{-2} of AuPt(I) catalyst system (b).

higher than that of Pt catalyst together with higher open circuit potential (OCV). Additionally, AuPt(I) catalyst generates a higher maximum power density, which is about 130% higher than that of the Pt catalyst. Such an improved activity indicates that the use of AuPt alloy catalyst can lead to a substantial reduction of Pt catalyst quantities in the fuel cell. Actually, the amount of Pt in the AuPt(I) is 0.4 mg cm^{-2}, about only 10-20% of the commercial catalyst.[13-16] Additionally, a stability test at constant current (100 mA cm^{-2}) was also conducted as shown in Fig. 6(b). Sustainable performance was obtained, although the absolute power value was lower than that of a state-of-art catalyst. Detailed studies on the origins of the excellent performance of the carbon paper supported AuPt alloy catalyst will be reported in the near future.

4. Conclusions

The main morphological feature of AuPt catalysts prepared by potentiostatic deposition is a typical dendritic nanostructure, which can be accelerated by increased Au content. Based on the XRD, XPS and EDX analysis, AuPt alloy catalysts were synthesized as bimetallic alloys with 60-80% Au content and relatively small particle size of 15-20 nm. Furthermore, XPS analysis revealed that the role of Pt atoms as electron acceptors at sites with poor metallic coordination and consequent high oxygen coordination with an increase of Au content in AuPt alloy catalyst, results from the distinct electronic structure and significant surface effects due to their dendritic nanostructures. AuPt alloy catalyst with 60% Au content exhibits significantly high catalytic activity for formic acid electro-oxidation. Au atoms alloyed with Pt atoms in the AuPt alloy catalyst may have played an important role in either removing the formation of the intermediate CO-like species or providing oxygenated species more favorably for the complete electro-oxidation of formic acid. The excellent power performance of MEA composed of AuPt catalyst is due mainly to the superior catalytic activity for formic acid electro-oxidation and adequate electrode structure. Further, for earlier commercialization, a more profound study of catalyst reduction and durability test is underway.

Acknowledgements

References

1. J. Lipkowski and P.N. Ross, *Electrocatalysis*; Wiley-VCH: New York (1998).
2. W. Vielstich, *Fuel Cells; Modern Process for the Electro-chemical Production of Energy*; Wiley-Interscience: London (1965).
3. S. Nakabayashi, I. Yagi, N. Sugiyama, K. Tamura, and K. Uosaki, *Surf. Sci.*, **386**, 82 (1997).
4. S. Song and P. Tsiakaras, *Appl. Catal. B: Environ.*, **63**, 187 (2006).
5. S. Uhm, H.J. Lee, Y. Kwon, and J. Lee, *Angew. Chem. Int. Ed.*, **47**, 10163 (2008).
6. S. Kang, J. Lee, J.K. Lee, S.-Y. Chung, and Y. Tak, *J. Phys. Chem. B*, **110**, 7270 (2006).
7. S. Uhm, S.T. Chung, and J. Lee, *Electrochem. Commun.*, **9**, 2027 (2007).
8. S. Uhm, S.T. Chung, and J. Lee, *J. Power Sources*, **178**, 34 (2008).
9. S. Uhm, Y. Kwon, S.T. Chung, and J. Lee, *Electrochim. Acta*, **53**, 5162 (2008).
10. S. Uhm, H.J. Lee, and J. Lee, *Phys. Chem. Chem. Phys.*, **11**, 9326 (2009).
11. Y. Zhu, S. Ha, and R.I. Masel, *J. Power Sources*, **130**, 8 (2004).
12. X. Wang, J-M. Hu, and I-M. Hsing, *J. Electroanal. Chem.*, **562**, 73 (2004).
13. http://www.fuelcellmarkets.com/cabot/news_and_information/3,1,6270,1,13970.html
14. V. Baglio, A. Di Blasi, E. Modica, P. Cretì, V. Antonucci, and A.S. Aricò, *J. New Mat. Electrochem. Systems*, **9**, 41 (2006).
15. S. Ha, R. Larsen, and R.I. Masel, *J. Power Sources*, **144**, 28 (2005).
16. S. Ha, R. Larsen, Y. Zhu, and R.I. Masel, *Fuel Cells*, **4**, 337 (2005).
17. R. Larsen, S. Ha, J. Zakzeski, and R.I. Masel, *J. Power Sources*, **157**, 78 (2006).
18. E. Rach and J. Heitbaum, *Electrochim. Acta*, **32**, 1173 (1987).
19. L.D. Burke and B.H. Lee, *J. Electroanal. Chem.*, **330**, 637 (1992).
20. J. Xiang, B.-L. Wu, and S.-L. Chen, *J. Electroanal. Chem.*, **517**, 95 (2001).
21. G.L. Beltramo, T.E. Shubina, and M.T M. Koper, *Chem Phys Chem*, **5**, 2597 (2005).
22. J-H. Choi, K-J. Jeong, Y. Dong, J. Han, T-H. Lim, J-S Lee, and Y-E. Sung, *J. Power Sources*, **163**, 71 (2006).
23. J.K. Lee, J. Lee, J. Han, T-H. Lim, Y-E. Sung, and Y. Tak, *Electrochim. Acta*, **53**, 3474 (2008).
24. M. Eikerling, A.A. Kornyshev, and A.A. Kulikovsky, in: *Encyclopedia of Electrochemistry*, Vol. 5 (Eds. A. Bard, M. Stratmann, D. MacDonald) (2003).
25. M. Eikerling, A.S. Loselevich, and A.A. Kornyshev, *Fuel Cells*, **4**, 131 (2004).
26. E.J. Taylor, E.B. Anderson, and N.R.K. Vilambi, *J. Electrochem. Soc.*, **139**, L45 (1992).
27. F. Gloaguen, J.-M. Leger, and C. Lamy, *J. Appl. Electrochem.*, **27**, 1052 (1997).
28. O. Antoine and R. Durand, *Electrochem. Solid-State Lett.*, **4**, A55 (2001).
29. H. Natter and R. Hempelmann, *Electrochim. Acta*, **49**, 51 (2003).
30. S.L. Chen and A. Kucernak, *J. Phys. Chem. B*, **107**, 8392 (2003).
31. H. Kim, N.P. Subramanian, and B.N. Popov, *J. Power Sources*, **138**, 14 (2004).
32. C. Wang, M. Waje, X. Wang, J.M. Tang, R.C. Haddon, and Y. Yan, *Nano Lett.*, **4**, 345 (2004).
33. Z.D. Wei and S.H. Chan, *J. Electroanal. Chem.*, **569**, 23 (2004).
34. J. Lee, J. Seo, K. Han, and H. Kim, *J. Power Sources*, **163**, 349 (2006).
35. Z.D. Wei, S.G. Chen, Y. Liu, C.X. Sun, Z.G. Shao, and P.K. Shen, *J. Phys. Chem. C*, **111**, 15456 (2007).
36. A. Wieckowski, E.R. Savinova, and C.G. Vayenas, *Catalysis and Electrocatalysis at Nanoparticle Surface*; Marcel Dekker, Inc.: New York, Basel (2003).
37. V.M. Jovanovic, D. Tripkovic, A. Tripkovic, A. Kowal, and J. Stoch, *Electrochem. Commun.*, **7**, 1039 (2005).
38. A.R. Layson and M.R. Columbia, *Microchem. J.*, **56**, 103 (1997).
39. S. Toyama, O. Takei, M. Tsuge, R. Usami, K. Horikoshi, and S. Kato, *Electrochem. Commun.*, **4**, 540 (2002).
40. L.M. Plyasova, I.Y. Molina, A.N. Gavrilov, S.V. Cherepanova, O.V. Cherstiouk, N.A. Rudina, E.R. Savinova, and G.A. Tsirlina, *Electrochim. Acta*, **51**, 4477 (2006).
41. W.H. Lizcano-Valbuena, V.A. Paganin, C.A.P. Leite, F. Galembeck, and E.R. Gonzalez, *Electrochim. Acta*, **48**, 3869 (2003).
42. M. Carmo, V.A. Pagnin, J.M. Rosolen, and E.R. Gonzalez, *J. Power Sources*, **142**, 169 (2005).
43. D.V. Leff, P.C. Ohara, J.R. Heath, and W.M. Gelbart, *J. Phys. Chem.*, **99**, 7036 (1995).
44. J.D. Grunwaldt, C. Kiener, C. Wogerbauer, and A. Baiker, *J. Catal.*, **181**, 223 (1999).
45. W.F. Yan, V. Petkov, S.M. Mahurin, S.H. Overbury, and S. Dai, *Catal. Commun.*, **6**, 404 (2005).
46. J. Choi, K. Park, I. Park, K. Kim, J. Lee, and Y. Sung, *J. Electrochem. Soc.*, **153**, A1812 (2006).
47. H. Tang, J.H. Chen, Z.P. Huang, D.Z. Wang, Z.F. Ren, L.H. Nie, Y.F. Kuang, and S.Z. Yao, *Carbon*, **42**, 191 (2004).
48. Y.Y. Shao, G.P. Yin, J.J. Wang, Y.Z. Gao, and P.F. Shi, *J. Electrochem. Soc.*, **153**, 1261 (2006).
49. N. Toshima and T. Yonezawa, *New J. Chem.*, **22**, 1179 (1998).
50. S. Hufner and G. K. Wertheim, *Phys. Rev. B*, **11**, 678 (1975).
51. A.K. Shukla, A.S. Arico, K.M. El-Khatib, H. Kim, P.L. Antonucci, and V. Antonucci, *Appl. Surf. Sci.*, **137**, 20 (1999).

Sunghyun Uhm, Hongrae Jeon and Jaeyoung Lee

52. J. Knecht, G. Stark, and Frencius, *Z. Anal. Chem.*, **289**, 206 (1978).
53. Y.J. Huang, D. Li, and J.H. Li, *Chem. Phys. Lett.*, **389**, 14 (2004).
54. L. Qiu, F. Liu, L. Zhao, W. Yang, and J. Yao, *Langmuir*, **22**, 4480 (2006).
55. D.B. Laurence, *Gold Bull.*, **37**, 125 (2004).
56. H. Kita and H.W. Lei, *J. Electroanal. Chem.*, **388**, 167 (1995).
57. I. Becerik and F. Kadirgan, *J. Electrochem. Soc.*, **148**, D49 (2001).
58. D. Mott, J. Luo, P.N. Njoki, Y. Lin, L. Wang, and C-J. Zhong, *Catal. Today*, **122**, 378 (2007).
59. M. Uchida, Y. Aoyama, N. Eda, and A. Ohta, *J. Electrochem. Soc.*, **142**, 4143 (1995).
60. M. Uchida, Y. Aoyama, N. Eda, and A. Ohta, *J. Electrochem. Soc.*, **142**, 463 (1995).
61. E. Bosco, *J. Electroanal. Chem.*, **366**, 43 (1994).
62. E. Passalacqua, F. Lufrano, G. Squadrito, A. Patti, and L. Giorgi, *Electrochim. Acta*, **46**, 799 (2001).